A homozygous variant in *NDUFA8* is associated with developmental delay, microcephaly, and epilepsy due to mitochondrial complex I deficiency

Yukiko Yatsuka[1,2], Yoshihito Kishita[1,2], Luke E. Formosa[3], Masaru Shimura[4], Fumihito Nozaki[5], Tatsuya Fujii[5], Kazuhiro R. Nitta[1,2], Akira Ohtake[6,7], Kei Murayama[4], Michael T. Ryan[3], Yasushi Okazaki[1,2,8]

[1]Intractable Disease Research Center, Juntendo University, Bunkyo, Tokyo 113-8421, Japan
[2]Diagnostics and Therapeutics of Intractable Diseases, Graduate School of Medicine, Juntendo University, Bunkyo, Tokyo 113-8421, Japan
[3]Department of Biochemistry and Molecular Biology, Monash Biomedicine Discovery Institute, Monash University, Victoria 3800, Australia
[4]Department of Metabolism, Chiba Children's Hospital, Midori, Chiba 266-0007, Japan
[5]Department of Pediatrics, Shiga Medical Center for Children, Moriyama, Shiga 524-0022, Japan
[6]Center for Intractable Diseases, Saitama Medical University Hospital, Saitama 350-0495, Japan
[7]Department of Pediatrics & Clinical Genomics, Faculty of Medicine, Saitama Medical University, Saitama 350-0495, Japan
[8]Laboratory for Comprehensive Genomic Analysis, RIKEN Center for Integrative Medical Sciences, Yokohama, Kanagawa 230-0045, Japan

Corresponding author: Yasushi Okazaki
email: ya-okazaki@juntendo.ac.jp
Diagnostics and Therapeutics of Intractable Diseases,
Intractable Disease Research Center,
Graduate School of Medicine, Juntendo University,
Hongo 2-1-1, Bunkyo-ku, Tokyo 113-8421, Japan

Author contributions

YY, YK, and YO designed the study. Drafting of the manuscript was performed by YY. YY, YK, MS, and LF acquired data. YY and YK analyzed data. FN and TF provided the patient's clinical information. FN is the attending physician of the patient. KRN, AO, KM, MR and YO gave critical comments. YO led the project.

Acknowledgements

We thank Dr. Hiroyuki Miyoshi of Keio University and RIKEN Bio Resource Center for the CS-CA-MCS plasmid (#RDB05963). We also thank the Laboratory of Molecular and Biochemical Research,

Research Support Center, Juntendo University Graduate School of Medicine, for supporting the experiment.

This work was supported by grants of the “Practical Research Project for Rare/Intractable Diseases” [JP20ek0109468, JP19ek0109273], the “Program for an Integrated Database of Clinical and Genomic Information” [JP19kk0205014] and “Platform Program for Promotion of Genome Medicine” [JP20kk0305015] from the Japan Agency for Medical Research and Development (AMED) (http://www.amed.go.jp/en/), JSPS KAKENHI TypeB [19H03624], and also the MEXT-Supported Program for the Private University Research Branding Project. MR acknowledges funding from the NHMRC [1164459, 1107094].

Conflicts of interest

The authors declare no competing financial interests.

Data Availability

The data that support the findings of this study are available from the corresponding author upon reasonable request.

Ethics approval

This study was approved by the ethics committee of Juntendo University and was performed after receiving written informed consent from the parents of the patient.

Consent to participate

Written informed consent was obtained from the parents.

Consent for publication

Written informed consent was obtained from the parents.

Abstract

Mitochondrial complex I deficiency is caused by pathogenic variants in mitochondrial and nuclear genes associated with complex I structure and assembly. We report the case of a patient with NDUFA8-related mitochondrial disease.

The patient presented with developmental delay, microcephaly, and epilepsy. His fibroblasts showed apparent biochemical defects in mitochondrial complex I. Whole-exome sequencing revealed that the patient carried a homozygous variant in *NDUFA8*. His fibroblasts showed a reduction in the protein expression level of not only NDUFA8, but also the other complex I subunits, consistent with assembly defects. The enzyme activity of complex I and oxygen consumption rate were restored by

reintroducing wild-type *NDUFA8* cDNA into patient fibroblasts. The functional properties of the variant in *NDUFA8* were also investigated using *NDUFA8* knockout cells expressing wild-type or mutated *NDUFA8* cDNA. These experiments further supported the pathogenicity of the variant in complex I assembly. This is the first report describing that the loss of NDUFA8, which has not previously been associated with mitochondrial disease, causes severe defect in the assembly of mitochondrial complex I, leading to progressive neurological and developmental abnormalities.

Keywords

Mitochondrial disease

OXPHOS

Complex I deficiency

Mitochondrial intermembrane space

CX_9C motif

Disulfide relay import pathway

INTRODUCTION

Mitochondrial diseases are a clinically and genetically heterogeneous group of diseases that present with a wide variety of clinical symptoms and are caused by mutations in mitochondrial or nuclear genes. The prevalence of mitochondrial diseases is estimated to be 1 in 5,000–10,000 individuals [1, 2]. Muscular and neurological symptoms are common features of mitochondrial diseases, but mitochondrial dysfunction can affect any organ of the body at any age. So far, more than 350 genes encoded in both the mitochondrial and nuclear genomes have been reported to be associated with mitochondrial diseases [3, 4].

Within the inner mitochondrial membrane, multi-protein complexes carry electrons along four redox reactions (Respiratory Chain Complexes I–IV), resulting in the generation of a proton gradient that is required for ATP production via ATP synthase (Complex V). This entire process is known as oxidative phosphorylation (OXPHOS). Complex I (NADH:ubiquinone oxidoreductase) is the largest OXPHOS complex composed of 45 subunits and requires at least 15 assembly factors for proper construction [5]. Complex I deficiency is caused by defects of mitochondrial proteins encoded by more than 30 nuclear genes and 7 mitochondrial genes [6]. The most common abnormalities of complex I deficiency include basal ganglia and/or brainstem lesions, respiratory abnormalities, muscular hypotonia, failure to thrive, seizures, and lactic acidemia [7]. Complex I is composed of six structural modules (N, Q, ND1, ND2, ND4, and ND5) [5]. The ND1 module contains mitochondrially encoded *MT-ND1* and nuclear-encoded *NDUFA3*, *NDUFA8*, and *NDUFA13*/*GRIM19*. Comprehensive complex I analysis using a combination of gene knockout and proteomic analysis revealed the importance of the ND1 module for assembly and activity [8, 9]. *NDUFA8* knockout cells show not only abnormality of the ND1 module but also abnormalities of the N, ND2, and ND5 modules. Of the four genes of the ND1 module, *MT-ND1* and *NDUFA13* are reported to be disease-associated. Mutations in *MT-ND1* have been identified in patients with Leber hereditary optic neuropathy (LHON) (OMIM #535000) [10] and Mitochondrial myopathy, Encephalopathy, Lactic Acidosis, and Stroke-like episodes (MELAS) (OMIM #540000) [11]. Mutation in *NDUFA13/GRIM19* is reported to cause early-onset hypotonia, dyskinesia and sensorial deficiencies [12].

Here, we report the use of whole-exome sequencing (WES) to identify a patient harboring a homozygous variant in *NDUFA8*. Biochemical analysis of patient fibroblasts revealed extremely decreased levels of NDUFA8 protein, which led to defects in the assembly and activity of complex I. The expression of wild-type *NDUFA8* cDNA in patient fibroblasts restored complex I assembly, enzymatic activity, and oxygen respiration. In addition, assembly failure was observed when the mutant *NDUFA8* was expressed in *NDUFA8* knockout cells. Our data suggest the pathogenicity of the *NDUFA8* variant and the importance of NDUFA8 during complex I formation.

MATERIALS AND METHODS

Information on the cell culture, SDS-PAGE, blue native PAGE, immunoblotting, real-time quantitative PCR, and measurement of oxygen consumption rate is provided as Supplemental Information. The antibodies and primer set are listed in Table 1.

Whole-exome sequencing and variant calling pipeline

Detailed method is provided in the Supplemental Information. In brief, genomic DNA was extracted from peripheral blood lymphocytes of the patient. WES libraries were captured with the SureSelect Human All Exon V6 kit (Agilent Technologies). The detected variants were filtered with minor allele frequencies (MAFs) of >0.5% for dbSNP, 1KG, the Exome Aggregation Consortium (ExAC), the Genome Aggregation Database (gnomAD), ESP6500siv2, and 3.5KJPNv2 database from the Tohoku Medical Megabank Organization (ToMMo).

DipStick assay of complex I

Enzyme activity immunocapture assays were performed using a Complex I Enzyme Activity Dipstick Assay Kit (ab109720; Abcam), in accordance with the manufacturer's instructions. All cells were cultured under normal conditions. Then, total cell lysates were freshly prepared. Protein concentration was determined using the BCA Protein Assay Kit (Thermo Fisher Scientific). A total of 50 µg of each sample was used in quadruplicate for detecting the enzyme activity of complex I. The intensity of each band on dipsticks was quantified using ImageJ [13].

Respiratory chain enzyme activity analysis

Each complex-specific assay procedure was performed as described previously [14, 15]. In brief, cell pellets were washed in PBS and then resuspended in ice-cold MegaFb Buffer (250 mM sucrose, 2 mM Hepes pH 7.4, 0.1 mM EGTA). Resuspended cells were homogenized with a Potter–Elvehjem homogenizer with 10–30 strokes. The number of strokes was determined by microscopic observation. Homogenates were centrifuged at 600 × g and 4°C for 10 min. Mitochondria in supernatants were enriched by centrifugation at 14,400 × g and 4°C for 10 min, washed in hypotonic buffer (25 mM potassium phosphate pH 7.2, 5 mM magnesium chloride), resuspended in the same buffer, and frozen at −80°C. These samples were repeatedly frozen and thawed three times before use. Respiratory chain enzyme activities were measured using Cary300 (Agilent Technologies) and were calculated as activities per milligram of protein (nmol/min/mg). Protein concentration was determined using the BCA Protein Assay Kit (Thermo Fisher Scientific).

Complementation of NDUFA8 in patient fibroblasts

The *NDUFA8* gene was cloned in a CS-CA-MCS lentiviral vector with CAG promoter for mammalian

cell expression, C-terminal V5 tag, and blasticidin resistance gene, as previously reported [16]. The PCR primers listed in Table 1 were used, which have sequences from the vector at the 5′ end and the ORF of *NDUFA8* at the 3′ end. ViraPower Packaging vectors and pCA-CS-ORF (NDUFA8) vector were co-transfected into HEK293FT cells with Lipofectamine 2000 (#11668019; Thermo Fisher Scientific). Supernatant containing the viral particles was collected after 48 h of transfection. Collected virus was infected into patient fibroblasts with 4 µg of polybrene (H9268; Sigma) per milliliter of culture medium. NDUFA8-complemented patient fibroblasts were harvested after blasticidin (ant-bl-1; InvivoGen) selection for more than 2 months.

Complementation of NDUFA8 in NDUFA8 knockout cells

The NDUFA8 knockout cells and complementation assay for the knockout cells were as previously described [8]. The preparation of NDUFA8 and NDUFA8(Arg47Cys) (c.139 C>T) virus expression vector is described in the Supplemental Information. Retroviral supernatants were prepared from HEK293T cells transfected with pBABE-Puro plasmid [17] encoding the cDNA of interest together with pCMV-VSV-G (Addgene; 8454) and p-gag/pol (Addgene; 14887) helper vectors using Lipofectamine LTX (Invitrogen). Supernatants were collected after 48 h and filtered through a 0.45 µm low-protein-binding filter (Merck) [18]. NDUFA8 knockout cells were then infected with the retrovirus with the addition of 8 µg/mL polybrene for stable and constitutive expression of NDUFA8Flag or NDUFA8(Arg47Cys)Flag. Transduced cells were selected by the addition of 2 µg/mL puromycin. Expression was validated using SDS-PAGE and immunoblotting using Flag antibodies.

Statistics

Statistical analysis was performed by two-tailed Student’s test. A p value <0.05 was considered to be statistically significant.

RESULTS

Case report

The patient was born at the gestational age of 39 weeks as the third child to nonconsanguineous Japanese parents, with a birth weight of 1,714 g (−4.3 SD). Apgar score was 7 at 1 min and 8 at 5 min. There was no family history of mitochondrial disease. At 2 months of age, he showed poor weight gain. Increased muscle tone and opisthotonus gradually developed. At 3 months of age, his weight, height, and head circumference were 3,535 g (−3.6 SD), 52 cm (−4.3 SD), and 35 cm (−2.9 SD), respectively. High palate and right inguinal hernia were also observed. There were no abnormalities observed in brain computed tomography, chest X-ray, or liver function tests. G-band analysis revealed a normal karyotype. At 7 months of age, he could not lift his head and roll. At the age of 1 year and 3 months, his weight, height, and head circumference were 4,845 g (−5.3 SD), 61 cm (−6.5 SD), and 38.7 cm (−7.0 SD), respectively. He did not have head control or the ability to locomote. Cerebral atrophy and enlarged ventricles were observed on brain magnetic resonance imaging. At the age of 2 years, he exhibited severe growth and psychomotor retardation and hypertonia with rigidity and spasticity, resulting in severe quadriplegia.

Elevated plasma levels of lactate (16.3 mmol/L; normal range < 1.8) and pyruvate (0.50 mmol/L; normal range < 0.1) were observed. Elevated lactate (3.6 mmol/L; normal range < 2.3) and pyruvate in the cerebrospinal fluid (0.23 mmol/L; normal range < 0.09) were also observed. In addition, organic acid analysis revealed a large amount of lactic acid excretion in the urine.

Pyruvate dehydrogenase activity in cultured lymphocytes was normal. Histochemical analysis using muscle biopsy performed at 2 years showed no ragged-red fibers and normal cytochrome c oxidase reactivity. Screening of known mitochondrial DNA variants in the muscle at m.3243, m.3256, m.3260, m.3271, m.3303, m.4296, m.5703, m.8344, m.8356, and m.8993 showed normal findings. Screening of other variants by single-stranded conformation polymorphism did not show any abnormalities. Southern blotting of mitochondrial DNA showed no deletions.

Brain magnetic resonance imaging (MRI) at the age of 3 years did not show significant change compared with that taken at 1 year of age; however, at the age of 19 years, cerebellar atrophy and thinning of the body of the corpus callosum became evident (Fig. 1). Cerebral atrophy also progressed. The patient is currently 26 years old and has severe quadriplegia, failure to thrive, hypertonia, short stature, microcephaly, psychomotor retardation, and epilepsy. He is bedridden and under artificial respiratory management and tube feeding.

Complex I deficiency of mitochondrial respiratory chain

Since mitochondrial disease was strongly suspected from the above symptoms, skin biopsy was performed at the age of 24 years. Patient fibroblasts showed a decrease of enzymatic activity of complex I (Table 2), while muscle homogenate showed decreases of enzyme activity of complexes I,

III and IV at the age of 2 years (Table 2).

Blue native (BN)-PAGE and western blot analysis revealed a drastic decrease in the respiratory supercomplexes comprising complexes I ($CI/CIII_2/CIV$ and $CI/CIII_2$) as well as increase in the intensity of the band of complex III dimer ($CIII_2$) in patient fibroblasts (Fig. 2A). It showed that $CIII_2$ was not incorporated into a supercomplex and was present alone as a separate entity. SDS-PAGE and western blot analysis also showed decreases in the complex I subunits NDUFA9 and NDUFB8 in the total patient fibroblast lysate (Fig. 2B). Thus, the patient was biochemically diagnosed as having complex I deficiency.

Whole-exome sequencing revealed a homozygous variant in *NDUFA8* gene

A homozygous missense variant (NM_014222.2:c.139C>T:p.Arg47Cys) in the *NDUFA8* gene was found in the patient by WES. This variant is rare, with only one allele of it being found among a total of 251,432 alleles (0.0004%) in the gnomAD-database. Mutation prediction software evaluated this variant as deleterious; SIFT showed that it is “damaging (0.04)” and Mutation Taster “disease-causing (1.00).” There were no other prioritized variants from the WES data of the patient. The homozygous variant was confirmed to be present in the patient’s DNA and to have been inherited from each parent by Sanger sequencing (Fig. 3A). It was thought that the p.Arg47Cys variant could affect the formation of the disulfide bridge in NDUFA8 because it provides a new cysteine residue next to C46. C46 is one of two cysteines in the single CX_9C motif, which are important for localization of small cysteine-rich proteins into the intermembrane space (IMS) (Fig. 3B) [19].

To investigate the effect of the variant based on the NDUFA8 protein levels, we performed western blot analysis using total protein extracted from cultured fibroblasts. Although the mRNA expression level of *NDUFA8* was comparable to that of the control cell lines (Fig. 3C), NDUFA8 protein was drastically decreased in patient fibroblasts to a level close to the detection limit (Fig. 3D). NDUFA9 and NDUFB8 were also affected (Fig. 2B), but this was considered to be a secondary effect from the decreased NDUFA8 levels. Indeed, previous studies of patient fibroblasts harboring a homozygous pathogenic variant in *NDUFA13* also showed a drastic reduction of not only NDUFA13 but also NDUFA9 and NDUFB8 [12]. Furthermore, knockout of NDUFA8 in cultured cells also leads to strongly decreased levels of ND1 module subunits surrounding NDUFA8 [8].

To understand the molecular implications of the p.Arg47Cys mutation in more detail, we analyzed the structural contacts of NDUFA8 within complex I (Fig. 3E and 3F). Analysis of the ovine complex I structure [20] revealed that R47 of NDUFA8 (purple; indicated with the arrow) interacts with subunits NDUFA13 (green) and NDUFB5 (orange). Upon closer analysis, it was evident that the guanidino group of the arginine side chain undergoes salt-bridging interactions with D80 of NDUFA13 and D188 (the second last C-terminal residue) of NDUFB5. Substitution of R47 for a cysteine residue would abolish these stabilizing interactions, potentially leading to decreased stability of NDUFA8 and

disruption of complex I assembly. Based on the molecular and structural characterization, we conclude that the variant causes NDUFA8 instability, which impairs complex I assembly.

Complementation assay

To demonstrate that the variant in *NDUFA8* is indeed responsible for the phenotype observed in patient fibroblasts, we carried out complementation analyses in control and patient fibroblasts using lentiviral expression (Fig. 4A). The levels of complex I and supercomplexes containing it ($CI/CIII_2/CIV$, $CI/CIII_2$) in patient fibroblasts were also recovered by *NDUFA8* complementation (Fig. 4B and 4C). We found elevated complex III levels due to the lack of supercomplexes containing complex I, and these returned to the same level as in control fibroblasts after complementation (Fig. 4C). Analysis of the complex I activity was measured by two different assays: dipstick assay using total cell extracts (Fig. 4D) and spectrophotometric assay using mitochondrial extracts (Fig. 4E). The complementation of CI defect by transduction with NDUFA8 in patient fibroblasts was confirmed (Fig. 4B-E). Next, we investigated the cellular oxygen consumption rate (OCR) in patient and control fibroblasts. Basal OCR and ATP production in patient fibroblasts were significantly lower than those in control fibroblasts, but maximal OCR was almost normal (Fig. 4F). *NDUFA8* transduction into patient fibroblasts resulted in the rescue of basal OCR and ATP production. Furthermore, the maximal OCR could be upregulated in patient fibroblasts transduced with wild-type *NDUFA8*. These findings strongly suggest that the complex I deficiency of the patient fibroblasts was caused by the *NDUFA8* variant.

Functional characterization of *NDUFA8* variant in *NDUFA8* knockout cells

Human complex I is composed of 45 subunits including 14 core subunits and 31 accessory subunits. Quantitative proteomic analysis using knockout cell lines generated by gene editing revealed that 25 of 31 accessory subunits are strictly required for the assembly of complex I [8]. *NDUFA8* knockout cells, such as *NDUFS5* and *NDUFB7* which also have CX_9C motifs, exhibited severe assembly defects of complex I. To investigate the functional properties of the variant in *NDUFA8*, we expressed wild-type and mutated *NDUFA8* cDNA in *NDUFA8* knockout cells (Fig. 5A), and examined the status of mitochondrial complex I formation. *NDUFA8* knockout cells transduced with wild-type *NDUFA8* showed the recovery of NDUFA8 protein and complex I assembly, whereas mutated *NDUFA8* cDNA encoding the p.Arg47Cys variant failed to rescue mitochondrial complex I assembly in *NDUFA8* knockout cells (Fig. 5B). These experiments using *NDUFA8* knockout cells further substantiate the pathogenicity of p.Arg47Cys variant in complex I assembly.

DISCUSSION

We report the case of a patient with NDUFA8-related mitochondrial disease, exhibiting developmental delay, microcephaly. The patient has a homozygous p.Arg47Cys variant in *NDUFA8*, which causes mitochondrial complex I deficiency.

MRI analysis of the patient showed cerebellar atrophy and thinning of corpus callosum as characteristic features. While cerebellar atrophy is frequently observed in patients with complex I deficiency [21, 22], hypoplasia of corpus callosum is not normally observed in such cases, but is seen in patients with PDH deficiency or harboring mutations in genes encoding GFM1, MRPS22, and EARS2 [23]. Corpus callosal dysgenesis was recently identified in Leigh syndrome patients harboring an isolated complex I deficiency due to mutations in the complex I assembly factor *NDUFAF8* gene [24] Muscle biopsy was also performed in two of three patients, and showed no COX-deficient fibers, unremarkable staining in histochemical investigations including cytochrome C oxidase/succinate dehydrogenase, and modified Gomori trichrome. The findings in brain and muscle were similar to those in the NDUFA8 patient described here.

Although there have been no reports of mitochondrial disease caused by biallelic mutations in *NDUFA8*, it has been reported that the disease might be caused in combination with *NDUFS2* mutations [25]. In that previously reported case, the patient presented with severe neonatal hypotonia, dysmorphic features, epilepsy, and signs of brainstem involvement. The patient died at 2 months of age. Plasma lactate was intermittently high. The enzyme activity of complex I was reduced to 13% in skeletal muscle, but was normal in fibroblasts. In these previous studies, the variant (NM_014222.2: c.G325A:p.Glu109Lys) in *NDUFA8* was not located at a highly conserved residue. Furthermore, only a limited number of complex I genes were sequenced and the association of other genes could not be ruled out.

Patient fibroblasts showed a decrease of enzymatic activity of mitochondrial complex I, whereas muscle homogenate of the patient showed low activity of complexes III and IV in addition to complex I (Table 2). It has been reported that complex I deficiency was often observed in both fibroblasts and muscle tissue from a patient harboring pathological mutations in one of the nuclear-encoded genes of complex I, whereas other complex defects were occasionally observed in muscle but not in fibroblasts [26]. In our case, there are two possible explanations: one is a secondary decline of complexes III and IV following decline of complex I, and the other is a problem of quality control with the muscle specimen because it was obtained more than 20 years ago.

confirmation of pathogenicity of the variant was performed using patient skin fibroblasts with complex I deficiency. Respiratory complex I consists of 45 subunits, which include 14 core subunits and 31 accessory subunits as mentioned above. Some of these accessory subunits are also required to assemble correctly and serve as enzymes of the mitochondrial respiratory chain. Stroud *et al.* investigated the contribution of accessory subunits to the assembly and stability of complex I by

generating knockout cell lines for each subunit [8]. It was shown that pathogenic variants found in accessory subunits of complex I could be classified into two groups: “mild assembly defects” and “severe assembly defects.” In our experiments, secondary decreases of NDUFB8 and NDUFA9 following a marked decrease of NDUFA8 by a homozygous mutation were observed in the patient fibroblasts. Such assembly defects were similar to the findings in cases of patients with mutations in the *NDUFA13* gene [12], which can be characterized as “Severe Assembly Defects.” It has also been shown that NDUFA8 and NDUFA13 are required to assemble ND1 module, and if one of these has been eliminated, complex I assembly fails, which leads to complex I deficiency.

Structural analysis reveals that complex I is embedded in the mitochondrial inner membrane with NDUFA8 of the ND1 module, NDUFS5 of the ND2 module, NDUFB10 of the ND4 module, and NDUFB7 of the ND5 module, located in the mitochondrial intermembrane space (IMS) [27]. These IMS-located subunits have common CX_nC motifs as their tertiary structure forms intra-molecular disulfide bridges between CX_nC motifs [19]. While three of four of these IMS-localized subunits (NDUFA8, NDUFB7, and NDUFS5) have a twin CX_9C motif, NDUFB10 does not. However, NDUFB10 has an atypical $CX_6C/CX_{11}C$ motif. It has been reported that pathogenic mutations in NDUFB10 cause mitochondrial complex I deficiency [28]. Since these subunits lack a canonical mitochondrial targeting signal, they appear to be inserted directly into complex I from the IMS [29]. The import of these proteins into the IMS relies on a specific pathway called the disulfide relay MIA40/CHCHD4 import pathway [27], which catalyzes the oxidative folding required for CX_9C motif-containing proteins [30, 31]. It has been suggested that complex I subunits that have disulfide bonds serve as stabilizers of the membrane arm domain of this enzyme [32]. Thus, it has been considered that CX_9C motif is a critical feature for these IMS-localized proteins [19]. Habich *et al.* reported that decreased proteins initiate formation of a metastable disulfide-linked complex with MIA40/CHCHD4 in advance of translocation into IMS [33]. Furthermore, it has been found that, if this interaction does not result in productive oxidation, the substrate is released into the cytosol and degraded by the proteasome [33, 34]. We hypothesize that the mutant NDUFA8 with its R47C missense alteration, which adds an additional cysteine residue next to the required cysteine for disulfide bond formation, fails to productively oxidize and could therefore be presented to the proteasome for redox quality control and degradation. These lines of evidence show that factors affecting this pathway can cause human diseases. In the other two proteins that have a CX_9C motif, variants associated with the disease have been reported. One variant (NM_004552.3: c.286C>T:p.Pro96Ser) in *NDUFS5* was reported as a variant of uncertain significance (VUS), but it was a heterozygous “likely deleterious” nuclear variant found in pooled DNA derived from patients having complex I deficiency. The other variant (NM_004146.6: c.115A>T:p.Met39Leu) in *NDUFB7* was found in esophageal cancer, but was not related to complex I deficiency [35, 36]. To date, there

have been no reports of variants in the CX_9C motifs of complex I IMS proteins affecting the precise formation of disulfide bonds that would likely cause complex I deficiency .

REFERENCES

1. Murayama, K., et al., *Recent topics: the diagnosis, molecular genesis, and treatment of mitochondrial diseases.* J Hum Genet, 2019. **64**(2): p. 113-125.
2. Skladal, D., J. Halliday, and D.R. Thorburn, *Minimum birth prevalence of mitochondrial respiratory chain disorders in children.* Brain, 2003. **126**(Pt 8): p. 1905-12.
3. Rahman, J. and S. Rahman, *Mitochondrial medicine in the omics era.* The Lancet, 2018. **391**(10139): p. 2560-2574.
4. Stenton, S.L. and H. Prokisch, *Advancing genomic approaches to the molecular diagnosis of mitochondrial disease.* Essays Biochem, 2018. **62**(3): p. 399-408.
5. Formosa, L.E., et al., *Building a complex complex: Assembly of mitochondrial respiratory chain complex I.* Semin Cell Dev Biol, 2018. **76**: p. 154-162.
6. Fassone, E. and S. Rahman, *Complex I deficiency: clinical features, biochemistry and molecular genetics.* J Med Genet, 2012. **49**(9): p. 578-90.
7. Distelmaier, F., et al., *Mitochondrial complex I deficiency: from organelle dysfunction to clinical disease.* Brain, 2009. **132**(Pt 4): p. 833-42.
8. Stroud, D.A., et al., *Accessory subunits are integral for assembly and function of human mitochondrial complex I.* Nature, 2016. **538**(7623): p. 123-126.
9. Guerrero-Castillo, S., et al., *The Assembly Pathway of Mitochondrial Respiratory Chain Complex I.* Cell Metab, 2017. **25**(1): p. 128-139.
10. Riordan-Eva, P. and A.E. Harding, *Leber's hereditary optic neuropathy: the clinical relevance of different mitochondrial DNA mutations.* J Med Genet, 1995. **32**: p. 81-87.
11. Kirby, D.M., et al., *Mutations of the mitochondrial ND1 gene as a cause of MELAS.* J Med Genet, 2004. **41**(10): p. 784-9.
12. Angebault, C., et al., *Mutation in NDUFA13/GRIM19 leads to early onset hypotonia, dyskinesia and sensorial deficiencies, and mitochondrial complex I instability.* Hum Mol Genet, 2015. **24**(14): p. 3948-55.
13. Schneider, C.A., W.S. Rasband, and K.W. Eliceiri, *NIH Image to ImageJ: 25 years of image analysis.* Nat Methods, 2012. **9**(7): p. 671-5.
14. Kirby, D.M., et al., *Biochemical Assays of Respiratory Chain Complex Activity*, in *Mitochondria, 2nd Edition*. 2007. p. 93-119.
15. Spinazzi, M., et al., *Assessment of mitochondrial respiratory chain enzymatic activities on tissues and cultured cells.* Nat Protoc, 2012. **7**(6): p. 1235-46.
16. Kohda, M., et al., *A Comprehensive Genomic Analysis Reveals the Genetic Landscape of Mitochondrial Respiratory Chain Complex Deficiencies.* PLoS Genet, 2016. **12**(1): p. e1005679.
17. Morgenstern, J.P. and H. Land, *Advanced mammalian gene transfer: high titre retroviral*

vectors with multiple drug selection markers and a complementary helper-free packaging cell line. Trends in Genetics, 1990. **6**: p. 280.

18. Stroud, D.A., et al., *COA6 is a mitochondrial complex IV assembly factor critical for biogenesis of mtDNA-encoded COX2.* Hum Mol Genet, 2015. **24**(19): p. 5404-15.
19. Szklarczyk, R., et al., *NDUFB7 and NDUFA8 are located at the intermembrane surface of complex I.* FEBS Lett, 2011. **585**(5): p. 737-43.
20. Letts, J.A., et al., *Structures of Respiratory Supercomplex I+III2 Reveal Functional and Conformational Crosstalk.* Mol Cell, 2019. **75**(6): p. 1131-1146 e6.
21. Fernando Scaglia, L.J.C.W., Georgirene D. Vladutiu, and Jill V. Hunter, *Predominant Cerebellar Volume Loss as a Neuroradiologic Feature of Pediatric Respiratory Chain Defects.* American Society of Neuroradiology, 2005. **26**: p. 1675–1680.
22. Bricout, M., et al., *Brain imaging in mitochondrial respiratory chain deficiency: combination of brain MRI features as a useful tool for genotype/phenotype correlations.* J Med Genet, 2014. **51**(7): p. 429-35.
23. Lebre, A.S., et al., *A common pattern of brain MRI imaging in mitochondrial diseases with complex I deficiency.* J Med Genet, 2011. **48**(1): p. 16-23.
24. Alston, C.L., et al., *Bi-allelic Mutations in NDUFA6 Establish Its Role in Early-Onset Isolated Mitochondrial Complex I Deficiency.* Am J Hum Genet, 2018. **103**(4): p. 592-601.
25. Bugiani, M., et al., *Clinical and molecular findings in children with complex I deficiency.* Biochim Biophys Acta, 2004. **1659**(2-3): p. 136-47.
26. van den Heuvel, L.P., J.A. Smeitink, and R.J. Rodenburg, *Biochemical examination of fibroblasts in the diagnosis and research of oxidative phosphorylation (OXPHOS) defects.* Mitochondrion, 2004. **4**(5-6): p. 395-401.
27. Modjtahedi, N., et al., *Mitochondrial Proteins Containing Coiled-Coil-Helix-Coiled-Coil-Helix (CHCH) Domains in Health and Disease.* Trends Biochem Sci, 2016. **41**(3): p. 245-260.
28. Friederich, M.W., et al., *Mutations in the accessory subunit NDUFB10 result in isolated complex I deficiency and illustrate the critical role of intermembrane space import for complex I holoenzyme assembly.* Hum Mol Genet, 2017. **26**(4): p. 702-716.
29. Mimaki, M., et al., *Understanding mitochondrial complex I assembly in health and disease.* Biochim Biophys Acta, 2012. **1817**(6): p. 851-62.
30. Hofmann, S., et al., *Functional and mutational characterization of human MIA40 acting during import into the mitochondrial intermembrane space.* J Mol Biol, 2005. **353**(3): p. 517-28.
31. Riemer, J., M. Fischer, and J.M. Herrmann, *Oxidation-driven protein import into*

mitochondria: Insights and blind spots. Biochim Biophys Acta, 2011. **1808**(3): p. 981-9.

32. Zhu, J., et al., *Structure of subcomplex Ibeta of mammalian respiratory complex I leads to new supernumerary subunit assignments.* Proc Natl Acad Sci U S A, 2015. **112**(39): p. 12087-92.

33. Habich, M., et al., *Vectorial Import via a Metastable Disulfide-Linked Complex Allows for a Quality Control Step and Import by the Mitochondrial Disulfide Relay.* Cell Rep, 2019. **26**(3): p. 759-774 e5.

34. Mohanraj, K., et al., *Inhibition of proteasome rescues a pathogenic variant of respiratory chain assembly factor COA7.* EMBO Mol Med, 2019. **11**(5).

35. Calvo, S.E., et al., *High-throughput, pooled sequencing identifies mutations in NUBPL and FOXRED1 in human complex I deficiency.* Nat Genet, 2010. **42**(10): p. 851-8.

36. Agrawal, N., et al., *Comparative genomic analysis of esophageal adenocarcinoma and squamous cell carcinoma.* Cancer Discov, 2012. **2**(10): p. 899-905.

FIGURES AND TABLES

Fig. 1 Magnetic resonance imaging

T1-weighted image of brain MRI at the ages of 3 years (left) and 19 years (right). The body of the corpus callosum became thinner (arrow) and cerebellar atrophy (arrowhead) became evident during the intervening 16 years. Cerebral atrophy with ventricular dilatation also progressed (not shown).

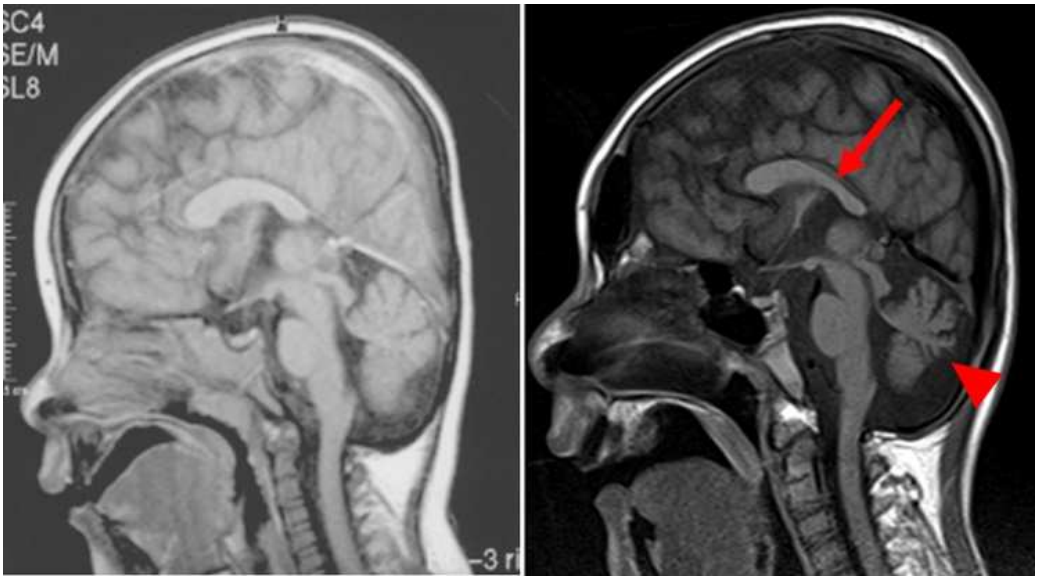

Fig. 2 Patient fibroblasts presented complex I deficiency

Biochemical analyses of mitochondrial respiratory chain complexes. (A) Blue native PAGE and western blot analyses of isolated and solubilized mitochondria from control and patient fibroblasts. Blots were probed with anti-NDUFA9 (for detection of CI/$CIII_2$, and CI/$CIII_2$/CIV), anti-UQCRC1 (for detection of CI/$CIII_2$/CIV, CI/$CIII_2$, $CIII_2$/CIV, and $CIII_2$), and anti-SDHA (for detection of complex II) antibodies. Succinate dehydrogenase complex subunit A (SDHA) protein of complex II was used as a loading control. CI/$CIII_2$ and CI/$CIII_2$/CIV were apparently decreased in patient fibroblasts. (B) SDS-PAGE and western blot analyses for subunits of complexes I–V in mitochondria isolated from control and patient fibroblasts. Anti-OXPHOS antibody cocktail, anti-NDUFA9 antibody, and anti-Hsp60 antibody were used for detection. Hsp60 was used as a loading control. CI defect was observed by two different antibodies.

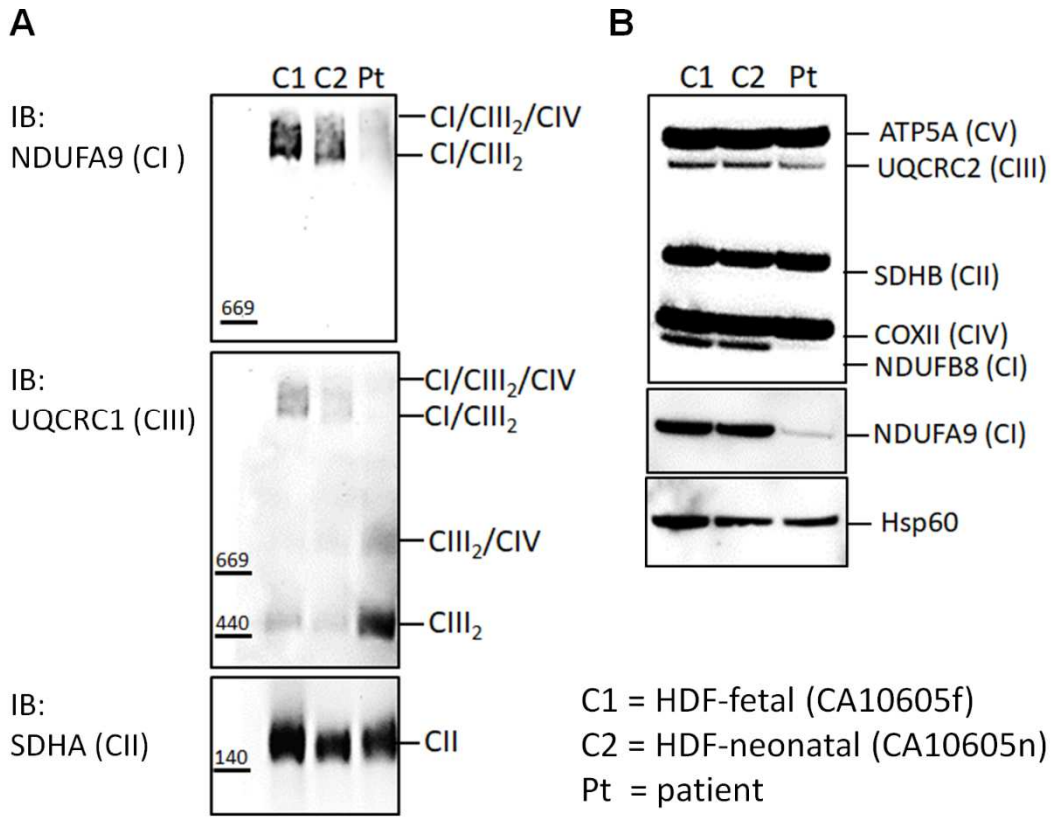

Fig. 3 Whole-exome sequencing revealed a missense variant in *NDUFA8* gene

A variant in *NDUFA8* and abundance of NDUFA8 protein in patient fibroblasts. (A) Sanger sequencing confirmed that the patient's father and mother were heterozygous for the variant in *NDUFA8*, whereas the affected patient was homozygous. (B) Interspecies alignment of the NDUFA8 and amino acid conservation around the CX_9C motif of NDUFA8 protein. (C) Expression level of *NDUFA8* mRNA was analyzed by quantitative RT-PCR using reverse-transcribed cDNA from the control and patient fibroblasts. The expression level of *NDUFA8* in the patient was thought to be comparable to that in the others. (D) NDUFA8 protein was analyzed by SDS-PAGE and western blotting in the total cell lysate of control and patient fibroblasts. The amount of NDUFA8 protein showed a profound decrease in the patient. (E) Molecular surface of complex I (light blue) highlighting the positions of NDUFA8 (purple, arrowhead), NDUFA13 (green), and NDUFB5 (orange) in complex I. IM, inner membrane; IMS, intermembrane space. PDB identifier: 6QA9. NDUFA8 indicated by a black arrowhead presents in IMS and interacts with other subunits of complex I: NDUFA13 and NDUFB5. (F) In terms of the molecular interactions of R47, there are salt-bridging interactions with D80 of NDUFA13 and D188 of NDUFB5. The closest disulfide bond is indicated in yellow.

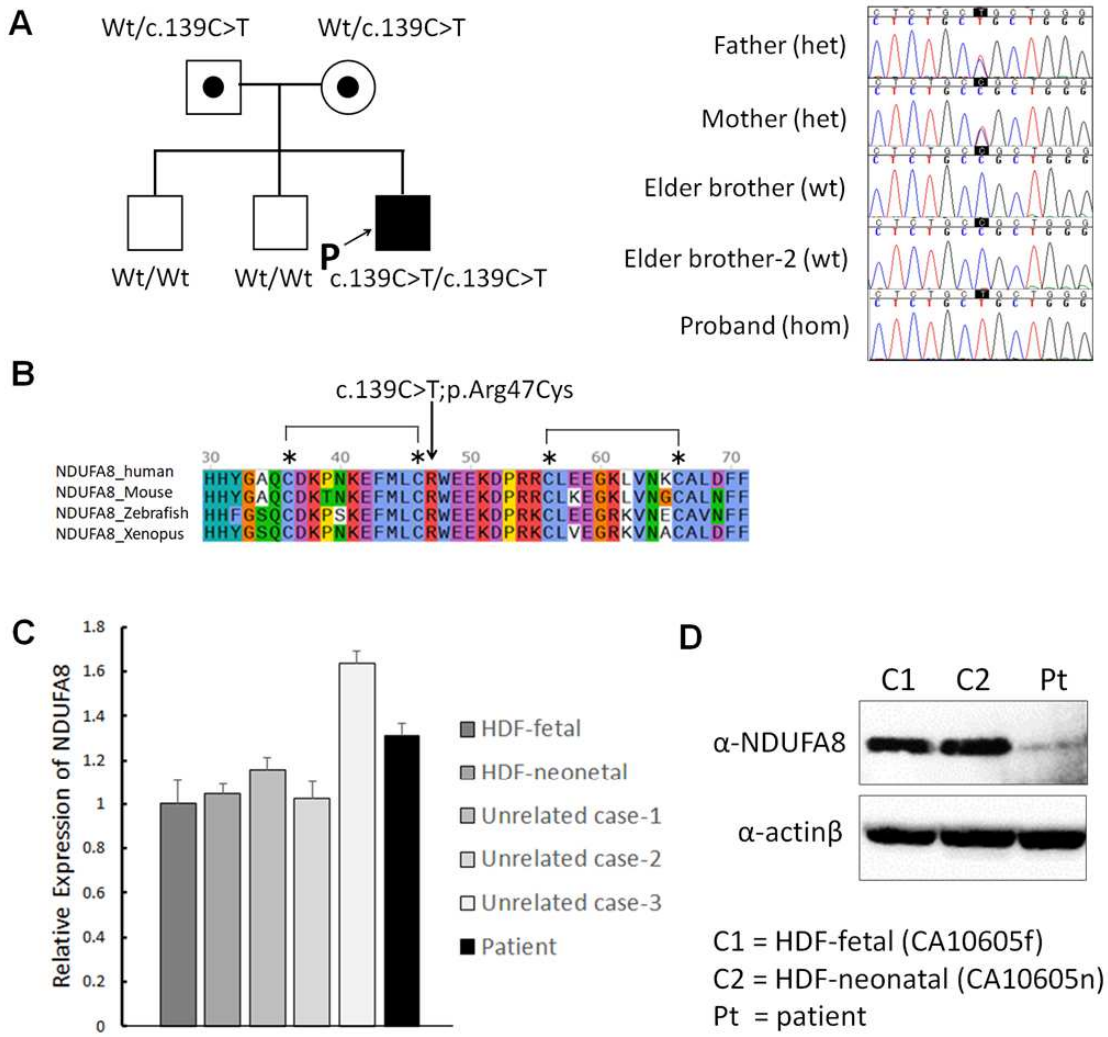
A
Wt/c.139C>T
Wt/c.139C>T
Wt/Wt
Wt/Wt
P
c.139C>T/c.139C>T
Father (het)
Mother (het)
Elder brother (wt)
Elder brother-2 (wt)
Proband (hom)
B
c.139C>T;p.Arg47Cys
NDUFA8_human
NDUFA8_Mouse
NDUFA8_Zebrafish
NDUFA8_Xenopus
C
Relative Expression of NDUFA8
HDF-fetal
HDF-neonetal
Unrelated case-1
Unrelated case-2
Unrelated case-3
Patient
D
C1
C2
Pt
α-NDUFA8
α-actinβ
C1 = HDF-fetal (CA10605f)
C2 = HDF-neonatal (CA10605n)
Pt = patient
E
Matrix
IM
IMS
NDUFA13
NDUFA8
NDUFB5
F
D80
R47
D188

508
509

Fig. 4 Complementation assay in patient fibroblasts

Lentivirus-mediated rescue of NDUFA8 in patient cells. (A) SDS-PAGE and western blot analyses of mitochondria from control and patient fibroblasts. Both cells overexpressed the wild-type *NDUFA8* or mitochondrially targeted V5-tagged TurboRFP (mtTurboRFP; negative control). SDS-PAGE and western blotting confirmed expression of NDUFA8 protein in patient fibroblasts transduced with *NDUFA8*. Hsp60 was used as a loading control. (B, C) Formation of respiratory chain complex I in control or patient fibroblasts transfected with *NDUFA8* cDNA was analyzed by BN-PAGE using two different detergents: 1% Triton (B) and 1% Digitonin (C). Immunoblotting was performed with anti-NDUFA9 (for detection of CI, CI/$CIII_2$, and CI/$CIII_2$/CIV), anti-UQCRC1 (for detection of CI/$CIII_2$/CIV, CI/$CIII_2$, $CIII_2$/CIV, and $CIII_2$), and anti-SDHA (for detection of complex II) antibodies. Complex II was used as the loading control. All CI-related complexes (CI, CI/III_2, and CI/$CIII_2$/CIV) were decreased in the patient. (D) Analysis of the complex I activity with Dipstick Assay Kit using total cell extracts from control and patient transduced with wild-type NDUFA8. The values represent the mean ± SD of four independent experiments. **p < 0.01 versus control. The complementation of CI defect by transduction with NDUFA8 in patient fibroblasts was confirmed. (E) Analysis of complex I activity with the spectrophotometric assays in mitochondrial extracts from control and patient transduced with wild-type NDUFA8. The values represent the mean ± SD of three independent experiments. **p < 0.01 versus control. In addition, in this assay, the complementation of CI defect by transduction with NDUFA8 in patient fibroblasts was confirmed. (F) Basal respiration rate, ATP production rate, and maximal respiration rate in control and patient fibroblasts with overexpression of *NDUFA8* or mtTurboRFP were analyzed by microscale oxygraphy. The results represent the mean ± SD of >8 technical replicates. **p < 0.01 versus control. Respiratory defects observed in microscale oxygraphy were complemented by transduction with NDUFA8 in patient fibroblasts.

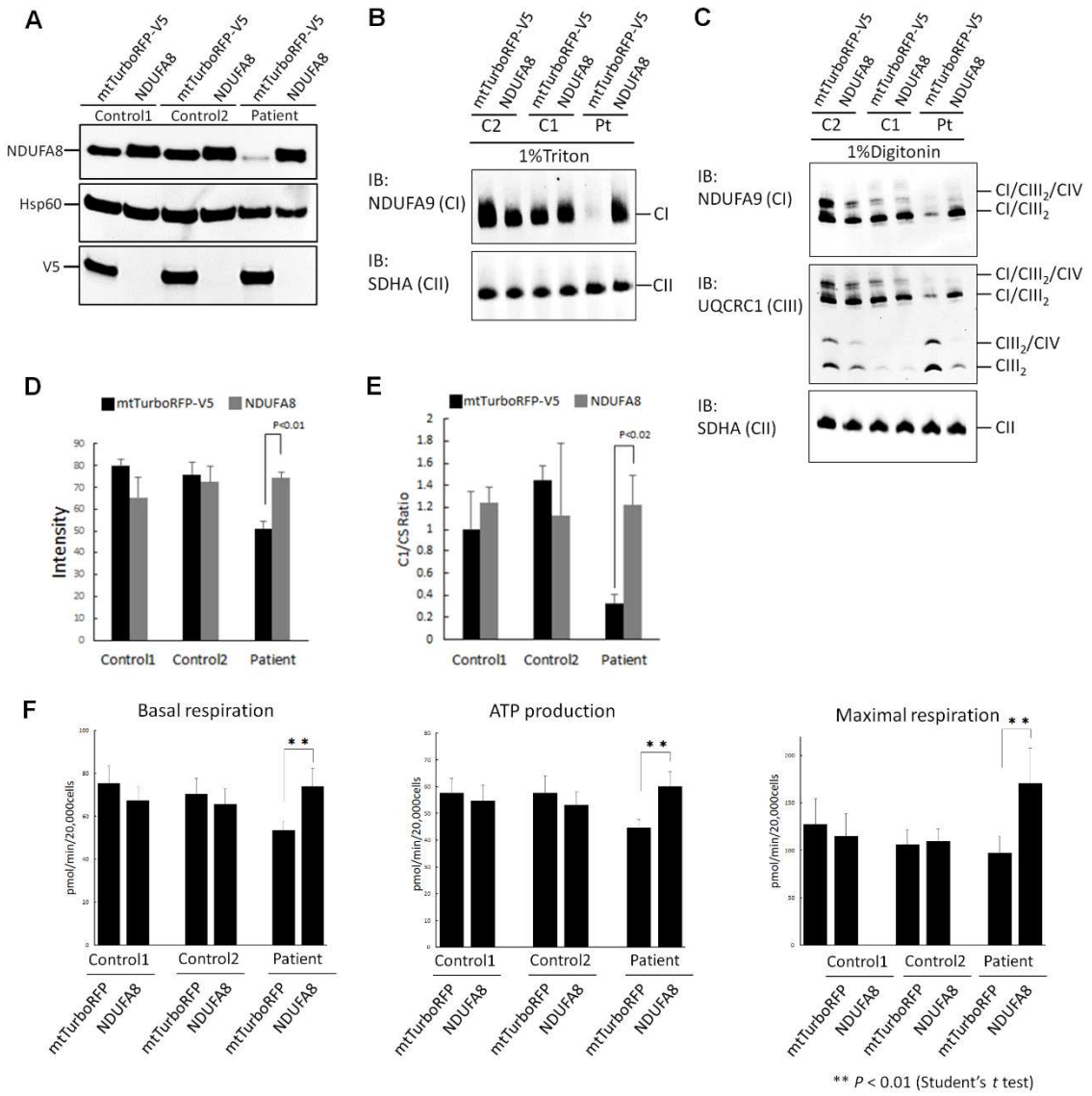
A
mtTurboRFP-V5
NDUFA8
Control1
Control2
Patient
NDUFA8
Hsp60
V5
B
C2
C1
Pt
1%Triton
IB:
NDUFA9 (CI)
CI
IB:
SDHA (CII)
CII
C
1%Digitonin
IB:
NDUFA9 (CI)
CI/CIII2/CIV
CI/CIII2
IB:
UQCRC1 (CIII)
CIII2/CIV
CIII2
IB:
SDHA (CII)
D
Intensity
P<0.01
E
C1/CS Ratio
P<0.02
F
Basal respiration
ATP production
Maximal respiration
pmol/min/20,000cells
** P < 0.01 (Student's t test)

534

535

Fig. 5 Complementation assay in NDUFA8 knockout cells

Complementation experiments in *NDUFA8* knockout cells. (A) NDUFA8 protein levels in *NDUFA8* knockout cells were transfected with the cDNA of Flag-tagged NDUFA8 encoding the p.Arg47Cys variant or wild-type were analyzed. SDS-PAGE and western blotting of total cell extracts were performed with anti-Flag and anti-SDHA antibodies. SDHA was used as a loading control. Overexpression of both p.Arg47Cys and wild-type Flag-tagged NDUFA8 was confirmed. (B) Formation of respiratory chain complex I and supercomplexes containing it ($CI/CIII_2/CIV$, $CI/CIII_2$) in control or *NDUFA8* knockout cells transfected with p.Arg47Cys or wild-type *NDUFA8* cDNA was analyzed by BN-PAGE. Immunoblotting was performed with anti-NDUFA9 for the detection of complex I and anti-SDHA antibodies for the detection of CII. CII was used as a loading control. Overexpressed wild-type NDUFA8 could complement a CI defect, but p.Arg47Cys NDUFA8 could not.

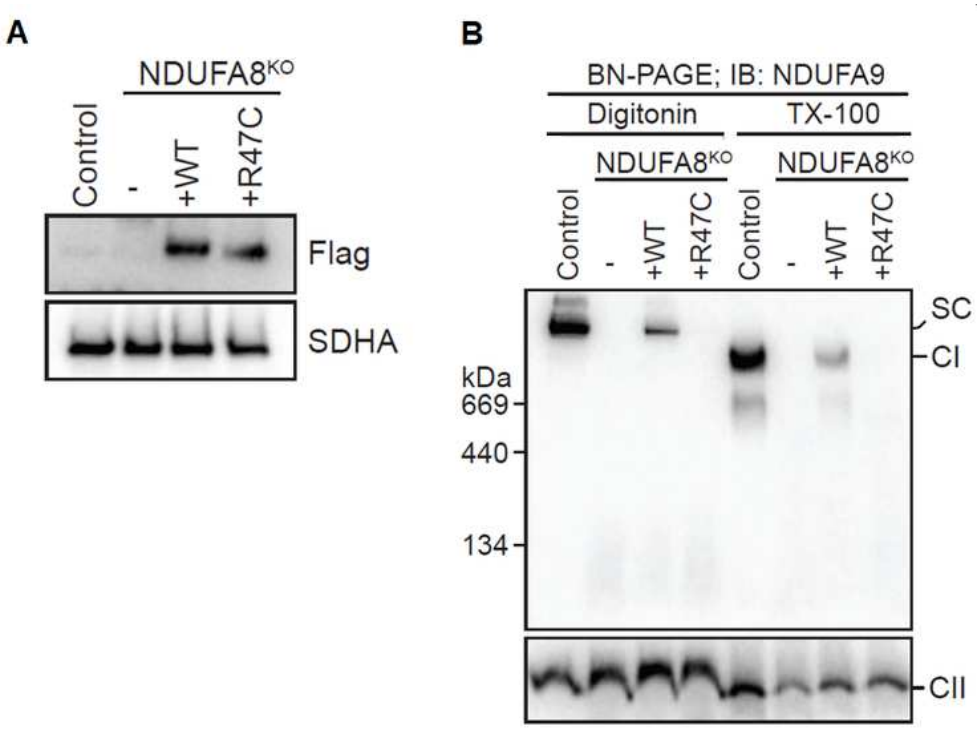

Table 1 Primer and antibody list

The list contains detailed information of the primers and antibodies used in this study.

Primer and Antibody List

Primers for direct sequencing of genomic DNA

name	detail	sequence
NDUFA8_V162L	chr9:124914453-124914475, GRCh37	5'-GCTGGCTGTTCACTTATTCATTT-3'
NDUFA8_V162R	chr9:124914810-124914787, GRCh37	5'-TTCTTGGTAAAGTCAGAACAGTGC-3'

Primers for real-time quantitative PCR

name	detail	sequence
NDUFA8-rt-F:	NM_014222, c.469G-c.489G	5'-GGAGAACTGTCAAAGGTCACC-3'
NDUFA8-rt-R:	NM_014222, c.577C-c.558T	5'-GCAGATCTCCCTCGATCTCA-3'
GAPDH-rt-F:	NM_002046, c.198A-c.217C	5'-ACTACATGGTTTACATGTTC-3'
GAPDH-rt-R:	NM_002046, c.395A - c.377G	5'-TCTCCATGGTGGTGAAGAC-3'

Primers for In-Fusion cloning

name	detail	sequence
NDUFA8-F	(Sequence from vector is underlined.)	5'-AGTGGCGGCCGCTCGAGCCACCATGCCGGGGATAGTGGAGC-3'
NDUFA8-R	(Sequence from vector is underlined.)	5'-TAGGCTTACCCTCGAGTTACTTGGTCCAGAAATAAAAGCGG-3'

Antibodies for immunoblotting

name	detail	
anti-NDUFA8	ab184952; Abcam	Fig.2-4
anti-β-actin	a5441; Sigma	Fig.2-4
anti-Hsp60	ab46798; Abcam	Fig.2-4
anti-OXPHOS cocktail	ab110411; Abcam	Fig.2-4
anti-NDUFA9	#459100; Thermo Fisher Scientific	Fig.2-4
anti-UQCRC1	#459140; Thermo Fisher Scientific	Fig.2-4
anti-NDUFA9	(generated in our lab)	Fig.5
anti-SDHA	ab14715; Abcam	Fig.5
anti-Flag M2 clone	F1804; Sigma Aldrich	Fig.5

Table 2 Spectrophotometric assay of patient specimens

Patient fibroblasts and muscle homogenate were evaluated for their enzymatic activity. Complex I activity was around one-quarter of that of the control.

Fibroblast	Patient	Control (n=35)
		Mean ± SD
	nmol/min/mg	nmol/min/mg
Complex I	18.5	74.9 ± 23.2
Complex II	91.5	56 ± 19.7
Complex III	20.1	12 ± 5.8
Complex IV	3.3	5.6 ± 2.1

Muscle homogenate	Patient	Control (n=5)
		Mean ± SD
	nmol/min/mg	nmol/min/mg
Complex I	64.3	257.2 ± 61.1
Complex II	399.5	345 ± 60.8
Complex III	55.1	235.7 ± 66.6
Complex IV	178.4	469.1 ± 94.3

Supporting Information

MATERIALS AND METHODS (Additional)

Cell culture

All cells were cultured at 37°C and 5% CO_2 in Dulbecco's modified Eagle's medium (DMEM) (#08458-45, Nacalai Tesque Inc.) supplemented with 10% fetal bovine serum (FBS-LE-12A; CAPRICORN) and 1% penicillin–streptomycin (#26253-84; Nacalai Tesque Inc.). Fetal human dermal fibroblasts (CA10605f, HDF-fetal; TOYOBO) was used as control-1. Neonatal human dermal fibroblasts (CA10605n, HDF-neonetal; TOYOBO) was used as control-2.

SDS-PAGE, blue native PAGE, and immunoblotting

To prepare the total cell lysate, cell pellets were lysed with 1× RIPA buffer (#08714-04; Nacalai Tesque) and kept on ice for 15 min. They were centrifuged at 10,000 g for 10 min at 4°C and the supernatants were collected. To prepare the mitochondrial fraction, cell pellets were suspended in mitochondrial isolation buffer A (220 mM mannitol, 20 mM HEPES, 70 mM sucrose, 1 mM EDTA, pH 7.4, 2 mg/ml bovine serum albumin, 1× protease inhibitor cocktail) and homogenized with a Potter–Elvehjem homogenizer as mentioned above. Then, homogenates were centrifugated at 700 g for 10 min at 4°C. The supernatants were collected into new tubes and centrifuged at 10,000 g for 10 min at 4°C. Mitochondrial pellets were washed twice with mitochondrial isolation buffer B (buffer A without bovine serum albumin). Protein concentration was determined by the BCA assay mentioned above. Isolated mitochondria were aliquoted at 20 μg each.

SDS-PAGE, BN-PAGE, and immunoblotting were performed as previously described [1]. The antibodies listed in Table 1 were used.

Real-time quantitative PCR

RNA was isolated from fibroblasts using TRIzol RNA Isolation Reagents (#15596018; Thermo Fisher Scientific) and then used for cDNA synthesis using SuperScript IV First-Strand Synthesis System (#18091200; Thermo Fisher Scientific) in accordance with the manufacturer's instructions. Synthesized cDNA was used as a template in real-time quantitative PCR with Power SYBR Green PCR Master Mix (#4368577; Thermo Fisher Scientific), which was performed on LightCycler 480 (Roche). The primer sets listed in Table 1 were used. Relative quantitation of *NDUFA8* expression level was performed using *GAPDH* for normalization.

Measurement of oxygen consumption rate

The oxygen consumption rate (OCR) of patient fibroblasts was measured by microscale oxygraphy (Seahorse XF96; Agilent Technologies). Cells were seeded at a density of 20,000 cells/well. After

measurement of the basal OCR, oligomycin, carbonyl cyanide-p-trifluoromethoxyphenylhydrazone (FCCP), and rotenone were added sequentially, and OCR was recorded after each addition. Maximum respiration rate (MRR) corresponds to the OCR after the addition of FCCP minus rotenone-insensitive OCR [2]. The data for each cell were normalized to the cell numbers determined using CyQUANT Cell Proliferation Kit (Invitrogen).

Whole-exome sequencing and variant calling pipeline

Genomic DNA was extracted from peripheral blood lymphocytes of the patient. WES libraries were captured with the SureSelect Human All Exon V6 kit (Agilent Technologies). WES was performed using 150-bp paired-end reads on a HiSeq4000 (Illumina). A bioinformatic filtering pipeline was modified from a previously described approach [1]. The quality of raw data was checked by FASTQC. After removing the low-quality reads, the adaptor reads were mapped to the reference genome (GRCh37/hg19) with Burrows–Wheeler Aligner (BWA), Picard, and SAMtools. GATK was also used for insertion and deletion realignment, quality recalibration, and variant calling. Detected variants were annotated using both ANNOVAR and custom Ruby scripts. After the selection of variants, PCR direct sequencing was performed, which aimed at validation and haplotype phasing of the variants using the primer set listed in Table 1. BigDye v3.1 cycle sequencing kit (Thermo Fisher Scientific) and Genetic Analyzer 3130xl (Thermo Fisher Scientific) were used for Sanger sequencing.

Retroviral expression vector construction

The NDUFA8 gene was disrupted using TALEN-mediated gene technology [3]. Sorted cells were subjected to screening using galactose containing DMEM to identify clonal populations that were not viable. Cells that were not viable in galactose medium were subsequently validated by sequencing of allelic indels and confirmation of protein loss by proteomic analysis [4]. The cDNA encoding human NDUFA8 was amplified from a cDNA library generated from HEK293T cells with primers that incorporated a C-terminal Flag tag. Mutant NDUFA8(Arg47Cys) (c.139 C>T) was prepared using overlapping mutagenic primers (together with the primers used to amplify wild-type NDUFA8) to generate two fragments, with each fragment incorporating the mutation required. PCR fragments were then cloned into the pBABE-puro retroviral plasmid (Addgene: 1764) [5] using Gibson Assembly (New England Biolabs) and the sequences were verified using Sanger sequencing.

REFERENCES

1. Kohda, M., et al., *A Comprehensive Genomic Analysis Reveals the Genetic Landscape of Mitochondrial Respiratory Chain Complex Deficiencies.* PLoS Genet, 2016. **12**(1): p.

631 e1005679.
632 2. Invernizzi, F., et al., *Microscale oxygraphy reveals OXPHOS impairment in MRC mutant*
633 *cells.* Mitochondrion, 2012. **12**(2): p. 328-35.
634 3. Reyon, D., et al., *FLASH assembly of TALENs for high-throughput genome editing.* Nat
635 Biotechnol, 2012. **30**(5): p. 460-5.
636 4. Stroud, D.A., et al., *Accessory subunits are integral for assembly and function of human*
637 *mitochondrial complex I.* Nature, 2016. **538**(7623): p. 123-126.
638 5. Morgenstern, J.P. and H. Land, *Advanced mammalian gene transfer: high titre retroviral*
639 *vectors with multiple drug selection markers and a complementary helper-free packaging*
640 *cell line.* Trends in Genetics, 1990. **6**: p. 280.
641